16. D. Lack, *Darwin's Finches* (Cambridge Univ. Press, Cambridge, 1947).
17. P. R. Grant, B. R. Grant, J. A. Markert, L. F. Keller, K. Petren, *Evol. Int. J. Org. Evol.* **58**, 1588 (2004).
18. P. R. Grant, B. R. Grant, K. Petren, *Am. Nat.* **166**, 56 (2005).
19. P. R. Grant, B. R. Grant, *Science* **313**, 224 (2006).
20. R. M. Zink, *Auk* **119**, 864 (2002).
21. I. Abbott, *J. Zool.* **184**, 119 (1978).
22. C. D. Ollier, *Z. Geomorphol.* **28**, 367 (1984).
23. R. C. Preece, K. D. Bennett, J. R. Carter, *J. Biogeogr.* **13**, 1 (1986).
24. K. J. Burns, S. J. Hackett, N. K. Klein, *Evol. Int. J. Org. Evol.* **56**, 1240 (2002).
25. See supporting material available on *Science* Online.
26. J. P. Roux, P. G. Ryan, S. J. Milton, C. L. Moloney, *Bothalia* **22**, 93 (1992).
27. P. G. Ryan, C. L. Moloney, J. Hudon, *Auk* **111**, 314 (1994).
28. P. G. Ryan, *Condor* **103**, 429 (2001).
29. P. G. Ryan, thesis, University of Cape Town, Cape Town, South Africa (1992).
30. The Administrator and Island Council of Tristan da Cunha gave permission to work at Tristan; C. Dorse, B. Watkins, Ovenstone Fishing, Tristan Natural Resources Department, and the South African Department of Environmental Affairs and Tourism gave field support. F. Joubert facilitated the use of a high-performance computing cluster (http://deepthought.bi.up.ac.za). The National Geographic Society, South African Department of Science and Technology, South African National Research Foundation, and University of Cape Town provided funding.

Supporting Online Material

www.sciencemag.org/cgi/content/full/315/5817/1420/DC1
Materials and Methods
SOM Text
Figs. S1 and S2
Tables S1 to S4
References

14 December 2006; accepted 25 January 2007
10.1126/science.1138829

Coupling Diurnal Cytosolic Ca^{2+} Oscillations to the CAS–IP_3 Pathway in *Arabidopsis*

Ru-Hang Tang,[1]* Shengcheng Han,[1]* Hailei Zheng,[2,3,1]* Charles W. Cook,[1] Christopher S. Choi,[1] Todd E. Woerner,[4] Robert B. Jackson,[1] Zhen-Ming Pei[1]†

Various signaling pathways rely on changes in cytosolic calcium ion concentration ($[Ca^{2+}]_i$). In plants, resting $[Ca^{2+}]_i$ oscillates diurnally. We show that in *Arabidopsis thaliana*, $[Ca^{2+}]_i$ oscillations are synchronized to extracellular Ca^{2+} concentration ($[Ca^{2+}]_o$) oscillations largely through the Ca^{2+}-sensing receptor CAS. CAS regulates concentrations of inositol 1,4,5-trisphosphate (IP_3), which in turn directs release of Ca^{2+} from internal stores. The oscillating amplitudes of $[Ca^{2+}]_o$ and $[Ca^{2+}]_i$ are controlled by soil Ca^{2+} concentrations and transpiration rates. The phase and period of oscillations are likely determined by stomatal conductance. Thus, the internal concentration of Ca^{2+} in plant cells is constantly being actively revised.

Organisms, from single-celled to multicellular, exploit the unique physical and chemical properties of the calcium ion to carry out essential biological functions. $[Ca^{2+}]_i$ increases transiently and/or repetitively in response to many abiotic and biotic stimuli (*1*–*3*) and also displays diurnal oscillations in animals and plants (*4*, *5*). In plants, the resting circadian $[Ca^{2+}]_i$ oscillations occur at the whole-tissue level (*6*), in contrast to those seen in specific neurons in animals (*4*, *7*), and are regulated by photoperiod and light intensity (*8*). This oscillating feature implies a robust regulatory machinery that synchronizes $[Ca^{2+}]_i$ throughout the plant. However, due to the lack of the knowledge of sensory receptors and Ca^{2+} channels (*2*, *5*, *9*), the underlying mechanisms for the resting $[Ca^{2+}]_i$ and its oscillations remain largely unknown.

We have cloned a receptor for external Ca^{2+} ($Ca^{2+}{}_o$), CAS, from *Arabidopsis* (*10*). CAS is expressed in the shoot, localizes to the plasma membrane, binds to Ca^{2+}, and mediates $Ca^{2+}{}_o$-induced $[Ca^{2+}]_i$ increases (CICI) in stomatal guard cells. We have generated *CAS* antisense lines (*CASas*) and shown that its mRNA and protein levels are reduced and that CICI is abolished (*10*). Identification of CAS and genetic manipulation of its activity may provide a powerful tool to dissect the mechanisms controlling $[Ca^{2+}]_i$ oscillations. We hypothesized not only that $Ca^{2+}{}_o$ serves as a signal triggering $[Ca^{2+}]_i$ increases, but also that $Ca^{2+}{}_o$ and CAS control the resting $[Ca^{2+}]_i$. To test this hypothesis, we measured the resting $[Ca^{2+}]_i$ using aequorin bioluminescence-based Ca^{2+} imaging (*6*, *8*, *11*) and found that the resting $[Ca^{2+}]_i$ was lower in *CASas* than in wild-type plants (Fig. 1A).

Next, we asked whether $[Ca^{2+}]_i$ oscillations were affected in *CASas*. Biological oscillations can be described by three parameters: amplitude, phase, and period (*12*). Quantitative analysis of leaf aequorin luminescence showed that the amplitudes of $[Ca^{2+}]_i$ oscillations were reduced in *CASas* throughout a long day (Fig. 1B; $P < 0.001$). The average resting $[Ca^{2+}]_i$ and absolute amplitude (peak − trough) were reduced by 46.0 ± 2.3% and 50.2 ± 3.5% ($P < 0.001$), respectively. However, the phase and period were not altered in *CASas* ($P > 0.1$), indicating that CAS is required for maintaining appropriate oscillating amplitudes. Similar results were seen in three *CASas* lines, *CASas1* to *CASas3* (*10*).

The reduced luminescence in *CASas* was not due to low abundance of cytosolic aequorin. Aequorin-expressing *CASas* lines were generated from a cross between *CASas* and a wild-type line carrying the *35S::aequorin* construct. The stability of aequorin expression in wild-type plants was confirmed for eight generations. The *CASas* and wild-type lines had similar aequorin protein levels (fig. S1A), which remained stable throughout a long day (fig. S1B). Finally, the maximum luminescence was identical in both genotypes, as estimated by discharge in excess Ca^{2+}.

Our data prompted us to investigate how $[Ca^{2+}]_o$ is regulated. Ca^{2+} is dissolved in water in the apoplast (extracellular spaces) and transported primarily from the root to the shoot through the transpiration stream (*13*, *14*). The transpiration rate is governed by stomatal conductance, which displays diurnal oscillations (*15*). We reasoned that $[Ca^{2+}]_o$ is synchronized to stomatal-conductance oscillations, and $[Ca^{2+}]_o$ oscillations are perceived by CAS and converted into $[Ca^{2+}]_i$ oscillations. Thus, the soil Ca^{2+}-signaling cascade would be as follows: soil Ca^{2+} → Ca^{2+} uptake and transport → $[Ca^{2+}]_o$ oscillations → CAS → $[Ca^{2+}]_i$ oscillations.

To test this hypothesis, we analyzed whether media Ca^{2+} affects $[Ca^{2+}]_i$. In wild-type plants, $[Ca^{2+}]_i$ was elevated with increases in media Ca^{2+}, whereas in *CASas* this response was reduced (Fig. 1C; $P < 0.001$). We monitored $[Ca^{2+}]_i$ oscillations in plants grown under physiological (1 mM) and elevated (30 mM) Ca^{2+} concentrations. The overall amplitudes of $[Ca^{2+}]_i$ were elevated in both wild-type and *CASas* plants with increases in media Ca^{2+}, but much more so in the wild type, although the phases were not altered (Fig. 1D).

We assessed how media Ca^{2+} regulates $[Ca^{2+}]_o$ and whether $[Ca^{2+}]_o$ oscillates. We monitored $[Ca^{2+}]_o$ directly by expressing aequorin in the apoplast as described previously (*16*). We found that $[Ca^{2+}]_o$ also displayed diurnal oscillations, which were similar in wild-type and *CASas* plants (Fig. 2A). $[Ca^{2+}]_o$ increased with increases in media Ca^{2+}, and both genotypes showed virtually identical responses (Fig. 2B). To ensure equivalent activity of apoplastic aequorin in both genotypes, we measured extracellular aequorin under conditions similar to those for cytosolic aequorin (*17*). The aequorin protein abundance was similar in wild-type and *CASas* plants (fig. S2).

[1]Department of Biology, Duke University, Durham, NC 27708, USA. [2]Department of Biology, Xiamen University, Xiamen, Fujian 361005, China. [3]State Key Laboratory of Marine Environmental Science, Xiamen University, Xiamen, Fujian 361005, China. [4]Department of Chemistry, Duke University, Durham, NC 27708, USA.

*These authors contributed equally to this work.
†To whom correspondence should be addressed. E-mail: zpei@duke.edu

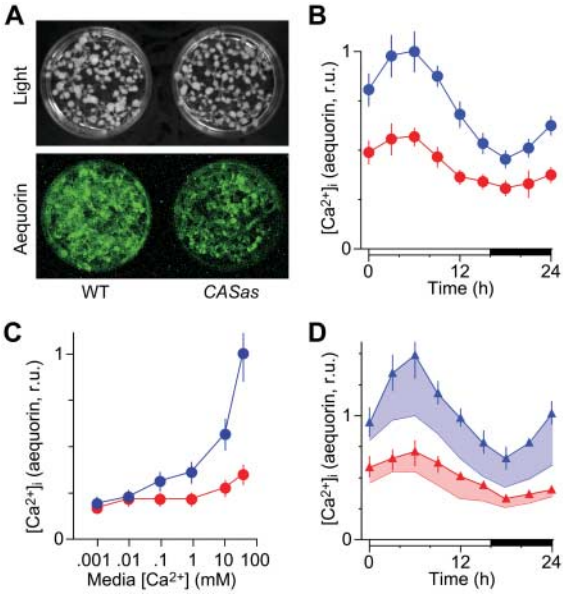

Fig. 1. Media Ca^{2+} and CAS control diurnal $[Ca^{2+}]_i$ oscillations. Blue, WT; red, *CASas*. (**A**) Imaging the resting $[Ca^{2+}]_i$ in *Arabidopsis* wild-type (WT) and *CAS* antisense (*CASas*). The bright light-field and aequorin luminescence images were taken at 8 hours after dawn from plants grown on ½ MS media under long-day conditions. (**B**) $[Ca^{2+}]_i$ oscillations in leaves. The aequorin luminescence images were taken from plants as in (A) every 3 hours starting from dawn. The luminescence was normalized to that discharged with excessive Ca^{2+}, and the maximum value was arbitrarily set to 1. The white and black bars represent objective light on and off, respectively. r.u., relative unit. Data from five separate experiments are shown [mean ± SD; n = 150 plants; two-way analysis of variance (ANOVA), $P < 0.001$]. (**C**) The effect of media Ca^{2+} on $[Ca^{2+}]_i$. Plants were grown on agar media containing varied $[Ca^{2+}]$ under long-day conditions for 2 to 3 weeks. Aequorin luminescence images were taken as in (B). Data from three experiments are shown (mean ± SD; n = 120 plants; two-way ANOVA, $P < 0.001$). (**D**) $[Ca^{2+}]_i$ oscillations in plants grown in 1 mM (solid lines) or 30 mM Ca^{2+} (triangles) (mean ± SD; n = 120 plants; two-way ANOVA, $P < 0.001$).

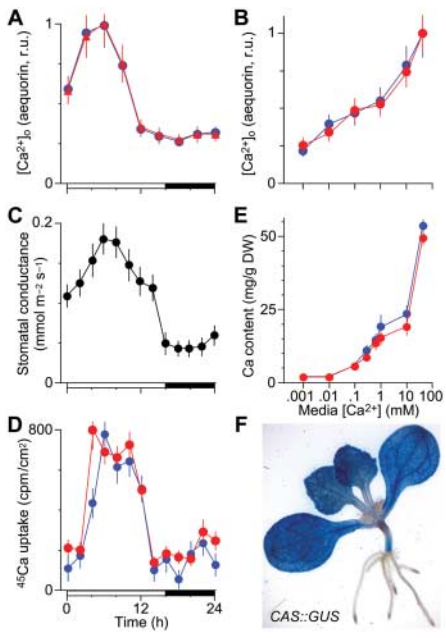

Fig. 2. Media Ca^{2+} and stomatal conductance control diurnal $[Ca^{2+}]_o$ oscillations. Blue, WT; red, *CASas*. (**A**) $[Ca^{2+}]_o$ oscillations in leaves. The luminescence images were taken every 3 hours, starting at dawn from plants expressing apoplastic aequorin grown on ½ MS. The luminescence was normalized to that discharged with excessive Ca^{2+}, and the maximum value was set to 1. Data from three separate experiments are shown (mean ± SD; n = 75 plants; two-way ANOVA, $P > 0.5$). (**B**) The effect of media Ca^{2+} on the resting $[Ca^{2+}]_o$. Luminescence images were taken as in Fig. 1C. The other conditions were the same as in (A). Data are shown as the mean ± SD (n = 75 plants; two-way ANOVA, $P > 0.5$). (**C**) WT plants were grown in soil for 3 weeks under long-day conditions, and stomatal conductance was monitored (mean ± SEM; n = 3). (**D**) ^{45}Ca uptake measured over a long day. ^{45}Ca was added to the growth solution at dawn. Shoots were collected every 2 hours for 2 days, and ^{45}Ca radioactivity was measured (*17*). The data for the second day are shown. cpm/cm^2, counts per minute/leaf area (cm^2). (**E**) The effect of media Ca^{2+} on the shoot Ca content in plants grown under conditions as in Fig. 1C. mg/g DW, milligrams Ca per gram dry weight (mean ± SD; n = 15 to 25 plants; two-way ANOVA, $P > 0.5$). (**F**) The analysis of *CAS promoter::GUS* reporter (*17*).

Finally, we determined whether stomatal-conductance oscillations are correlated with Ca^{2+} uptake and transport, $[Ca^{2+}]_o$ oscillations, and $[Ca^{2+}]_i$ oscillations. As expected, the stomatal conductance of wild-type plants was high in the day and low at night (Fig. 2C). We also found that wild-type and *CASas* plants displayed similar diurnal oscillations in ^{45}Ca uptake and transport (Fig. 2D). These experiments confirmed previous reports that Ca^{2+} uptake and transport to leaves are controlled mainly by transpiration that is regulated by stomatal conductance (*13*, *14*). The shoot Ca content of seedlings grown at various concentrations of media Ca^{2+} was similar between wild-type and *CASas* plants (Fig. 2E). Thus, the reduced $[Ca^{2+}]_i$ oscillations in *CASas* were due not to reduced Ca content, but rather to a defect in $Ca^{2+}{}_o$ sensing.

It appears that the phases and periods of oscillations in stomatal conductance, ^{45}Ca uptake, $[Ca^{2+}]_o$, and $[Ca^{2+}]_i$ were well correlated. CAS seems to control the amplitude of $[Ca^{2+}]_i$ oscillations, but not Ca uptake or $[Ca^{2+}]_o$ oscillations. Media Ca^{2+} concentration regulates the oscillating amplitudes of both $[Ca^{2+}]_o$ and $[Ca^{2+}]_i$. In addition, the expression patterns of CAS, noticeably in mesophyll cells and vascular tissues in the shoot (Fig. 2F), fit well with the route of Ca^{2+} transport and distribution in the shoot (*17*), supporting the function proposed for CAS.

Next, we asked how CAS couples $[Ca^{2+}]_i$ with $[Ca^{2+}]_o$, i.e., whether CAS mediates Ca^{2+} influx or release from internal stores. In animals, although diurnal $[Ca^{2+}]_i$ oscillations at the whole-tissue level have not been observed (*4*, *7*), fast $[Ca^{2+}]_i$ spiking at the cellular level has been well studied (*1*). External signals are perceived by cell-surface receptors, which activate phospholipase C (PLC), increasing inositol 1,4,5-trisphosphate (IP_3) concentration. IP_3 activates IP_3 receptors (IP_3Rs) in the endoplasmic reticulum (ER), resulting in Ca^{2+} release. The Ca^{2+} ions are reabsorbed by the ER, leading to $[Ca^{2+}]_i$ oscillations. In plants, although cell-surface receptors and IP_3Rs are unknown (*18*), it is possible that CAS might serve as a receptor triggering Ca^{2+} release. To explore this possibility, we investigated the function of CAS in CICI in a heterologous system as well as in planta.

CAS confers CICI in human embryonic kidney 293 (HEK293) cells (*10*). We observed that the CAS–green fluorescent protein (GFP) was localized in the vicinity of the plasma membrane in HEK293 cells (Fig. 3A), consistent with the subcellular localization in plants (*10*). We found that $Ca^{2+}{}_o$ triggered IP_3 production in *CAS*-expressing HEK293 cells (Fig. 3B). The PLC blockers, neomycin and U-73122, inhibited CICI (Fig. 3C). These results indicate that CAS can function as a receptor in the IP_3 pathway in HEK293 cells.

Next, we assessed whether CAS also serves as a receptor in the putative IP_3 pathway in *Arabidopsis*. In plants, some of the components seen in the animal IP_3 pathways have been identified (*17*, *18*). For instance, increases in IP_3 have been detected in response to several stimuli, which enhance the activities of PLCs. High-affinity IP_3 binding sites in internal membranes have been detected, although it is not clear whether plants have IP_3Rs. IP_3 can also trigger Ca^{2+} release from internal stores. Nonetheless, the molecular nature of corresponding cell-surface receptors remains obscure.

We found that neomycin abolished CICI in *Arabidopsis* guard cells (Fig. 3D). Similarly, we observed CICI in mesophyll cells and also detected CICI in intact leaves using aequorin imaging, which suggests that CICI occurs in cells other than guard cells and at the whole-leaf level. To analyze further whether IP_3 participates in CICI, we measured the IP_3 content of leaves. $Ca^{2+}{}_o$ induced IP_3 generation (Fig. 3E; $P < 0.01$), and neomycin eliminated the IP_3 production (Fig. 3F; $P > 0.5$). Together, these results suggest that $Ca^{2+}{}_o$ may evoke the IP_3 pathway in *Arabidopsis*.

To verify $Ca^{2+}{}_o$-induced IP_3 production, we carried out single-cell imaging of IP_3. The com-

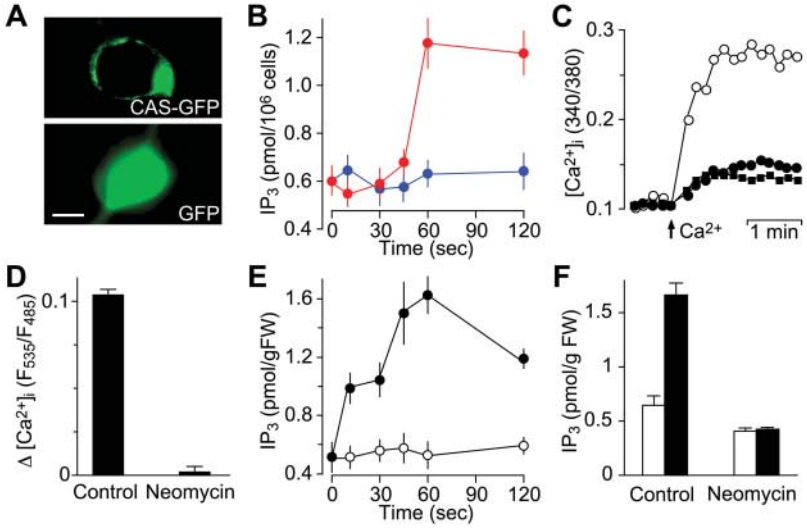

Fig. 3. CAS is a cell-surface receptor in the IP_3 pathway. (**A**) Plasma membrane localization of CAS in HEK293 cells expressing a *CAS-GFP* construct (upper) with GFP as a control (lower). Scale bar, 5 μm. (**B**) The effect of $Ca^{2+}{}_o$ on IP_3 generation in HEK293 cells expressing *CAS* (red). The control (blue) was cells transfected with empty vector. Cells were bathed in 0.1 mM Ca^{2+} before addition of 2.5 mM Ca^{2+} and harvested at the times indicated. The IP_3 content was determined by [^{3}H]IP_3 radioreceptor assay (*17*) (mean ± SEM; $n = 6$). (**C**) Inhibition of ClCl by PLC blockers in HEK293 cells expressing *CAS*. Cells were incubated with 0.1 mM Ca^{2+} without (white circles) or with 100 μM neomycin (black circles) or U-73122 (black squares) before Ca^{2+} stimulation. Ca^{2+} at 2.5 mM was added at the time indicated (arrow), and $[Ca^{2+}]_i$ was monitored by Fura-2 imaging (*17*). (**D**) Inhibition of ClCl by neomycin in guard cells. Epidermal peals carrying the Ca^{2+}-indicator cameleon were incubated in solution containing 50 μM Ca^{2+} for 2 hours, and then treated with 2.5 mM Ca^{2+} (*10*). Neomycin (100 μM) was added 15 min before addition of Ca^{2+}. $[Ca^{2+}]_i$ is shown as changes in emission fluorescence ratios ($\Delta[Ca^{2+}]_i$; $n = 15$ cells; $P < 0.001$). (**E**) $Ca^{2+}{}_o$ induces IP_3 generation in *Arabidopsis* leaves. Leaves were incubated in the solution containing 50 μM Ca^{2+} for 2 hours, then transferred to the same solution (white circles) or the solution containing 10 mM Ca^{2+} (black circles), and harvested at the times indicated. IP_3 was determined by [^{3}H]IP_3 assay (mean ± SEM; $n = 6$). (**F**) Neomycin inhibits $Ca^{2+}{}_o$-induced IP_3 generation in leaves. The samples were collected before addition of Ca^{2+} (white bars) or 60 s after addition of 10 mM Ca^{2+} (black bars). Neomycin (100 μM) was added 15 min before Ca^{2+} stimulation (mean ± SEM; $n = 6$). pmol/gFW, picomole per gram fresh weight.

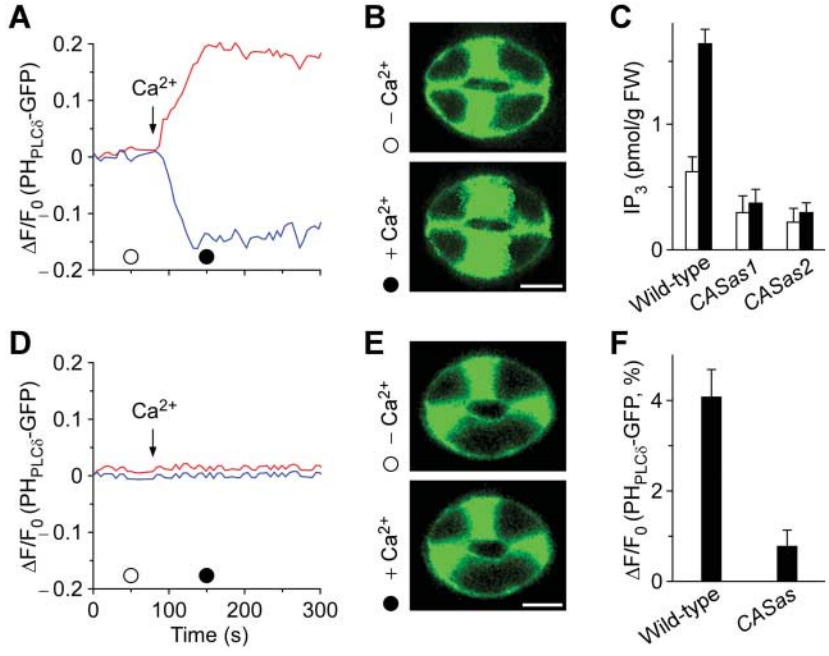

Fig. 4. CAS is required for the $Ca^{2+}{}_o$-evoked IP_3 pathway. (**A** and **B**) $Ca^{2+}{}_o$-induced IP_3 production in single WT guard cells. The leaf epidermis was incubated with 50 μM Ca^{2+} and treated with 10 mM Ca^{2+}. $Ca^{2+}{}_o$ triggered *$PH_{PLC\delta}$-GFP* translocation from the plasma membrane (blue) to the cytosol (red). The images in (B) correspond to before (○) and after (●) Ca^{2+} stimulation in (A). (**C**) IP_3 content in WT and *CASas* leaves with (black bars) and without (white bars) addition of 10 mM Ca^{2+} (mean ± SEM; $n = 6$; $P < 0.02$ for WT; $P > 0.5$ for *CASas1* and *CASas2*). (**D** and **E**) Defect in $Ca^{2+}{}_o$-induced IP_3 generation in *CASas* guard cells. The *CASas* line expressing *$PH_{PLC\delta}$-GFP* was generated from a cross between *CASas* and the wild-type *$PH_{PLC\delta}$-GFP* line, as in (A). (**F**) Increases in $PH_{PLC\delta}$-GFP fluorescence in the cytosol with addition of Ca^{2+} were analyzed from experiments as in (A) and (D). Thirty-eight out of 133 guard cells (28.6%) for the wild type (A) and 4 out of 76 (5.3%) for *CASas* (E) showed increases. Data are shown as the mean ± SEM ($P < 0.001$). Scale bars, 5 μm.

monly used biosensor for IP_3 is the PLC-δ1 pleckstrin homology domain fused to GFP ($PH_{PLC\delta}$-GFP), which binds phosphatidylinositol-4,5-bisphosphate (PIP_2) and IP_3 (*19*, *20*). Without stimulation, $PH_{PLC\delta}$-GFP is located mainly at the plasma membrane, whereas upon PIP_2 hydrolysis and formation of IP_3, $PH_{PLC\delta}$-GFP binds to IP_3, dissociates from the membrane, and translocates to the cytosol. This translocation can be used as an indicator of IP_3 (*21*–*23*). We generated *Arabidopsis* lines expressing *35S::$PH_{PLC\delta}$-GFP* and observed that $PH_{PLC\delta}$-GFP was localized primarily to the plasma membrane (fig. S3). Ca^{2+} triggered a reduction of $PH_{PLC\delta}$-GFP fluorescence in the plasma membrane but an elevation in the cytosol (Fig. 4, A and B), indicating an increase in IP_3 concentration.

To substantiate whether CAS is involved in the IP_3 pathway, we analyzed $Ca^{2+}{}_o$-induced IP_3 production in *CASas*. Both biochemical and single-cell imaging analyses showed that *CASas* was impaired in $Ca^{2+}{}_o$-induced IP_3 production (Fig. 4, C to F). These results suggest that CAS may act as a receptor in the IP_3 pathway, although CAS differs from its animal counterparts, the G protein–coupled receptors and receptor tyrosine kinases (*1*, *17*). Note that, because plant PLCs contain Ca^{2+} binding motifs, and are activated by Ca^{2+} (*24*), it is also possible that PLCs are activated by stimulus-triggered $[Ca^{2+}]_i$ increases rather than by cell-surface receptors. Characterization of the relation between CAS and PLCs will allow us to address this possibility.

We have revealed that $[Ca^{2+}]_i$ oscillations are coupled to the $[Ca^{2+}]_o$ oscillations–CAS–IP_3 pathway. Our data, together with previous studies, may explain how $[Ca^{2+}]_i$ oscillations are determined: the amplitude by the soil Ca^{2+} level and stomatal conductance, and the phase and period largely by stomatal-conductance oscillations. We can simulate $[Ca^{2+}]_i$ oscillations using a schematic model (fig. S4). First, CAS and a Ca^{2+}-influx channel, such as guard cell ICa (*25*), perceive $[Ca^{2+}]_o$ and convert it into $[Ca^{2+}]_i$. Second, $[Ca^{2+}]_o$ oscillates. The $[Ca^{2+}]_o$ is determined by two opposite processes: supplying fresh Ca^{2+} to the apoplast and sequestrating it into stores. For the sequestration, fresh Ca^{2+} ions bind

to newly synthesized cell-wall components, form Ca^{2+} oxalate, or move into internal stores (*13*, *14*). Most sequestrated Ca^{2+} ions become immobile, and thus continuous Ca^{2+} supplies are needed and likely to be the regulated step. Third, the stomatal-conductance oscillations are regulated by photoperiod and the clock (*15*). Finally, soil Ca^{2+} is the primary source controlling the amplitudes of $[Ca^{2+}]_i$ oscillations. Our findings may also revise further the concept of resting $[Ca^{2+}]_i$ in plants. The constant remodeling includes oscillations at the basal concentration of ~0.1 μM (*6*), similar to that in specific neurons (*4*, *7*), and shifts of this level according to soil Ca^{2+} status and CAS activity. Clearly, transpiration-mediated soil Ca^{2+} uptake and transport synchronize the resting $[Ca^{2+}]_i$ throughout the plant. Because the transpiration rate is regulated by numerous factors (*26*) and because soil Ca^{2+} levels can fluctuate throughout the year in nature (*27*), this soil Ca^{2+}-CAS-IP_3 pathway may be physiologically relevant (*17*).

References and Notes

1. M. J. Berridge, M. D. Bootman, H. L. Roderick, *Nat. Rev. Mol. Cell Biol.* **4**, 517 (2003).
2. A. M. Hetherington, C. Brownlee, *Annu. Rev. Plant Biol.* **55**, 401 (2004).
3. H. Knight, M. R. Knight, *Trends Plant Sci.* **6**, 262 (2001).
4. C. S. Colwell, *Eur. J. Neurosci.* **12**, 571 (2000).
5. A. N. Dodd, J. Love, A. A. Webb, *Trends Plant Sci.* **10**, 15 (2005).
6. C. H. Johnson *et al.*, *Science* **269**, 1863 (1995).
7. M. Ikeda *et al.*, *Neuron* **38**, 253 (2003).
8. J. Love, A. N. Dodd, A. A. Webb, *Plant Cell* **16**, 956 (2004).
9. D. Sanders, J. Pelloux, C. Brownlee, J. F. Harper, *Plant Cell* **14**, S401 (2002).
10. S. Han, R. Tang, L. K. Anderson, T. E. Woerner, Z.-M. Pei, *Nature* **425**, 196 (2003).
11. M. R. Knight, A. K. Campbell, S. M. Smith, A. J. Trewavas, *Nature* **352**, 524 (1991).
12. C. R. McClung, *Plant Cell* **18**, 792 (2006).
13. P. K. Hepler, *Plant Cell* **17**, 2142 (2005).
14. P. J. White, M. R. Broadley, *Ann. Bot. (London)* **92**, 487 (2003).
15. A. A. R. Webb, *New Phytol.* **160**, 281 (2003).
16. D. Gao, M. R. Knight, A. J. Trewavas, B. Sattelmacher, C. Plieth, *Plant Physiol.* **134**, 898 (2004).
17. Materials and methods are available as supporting material on *Science* Online.
18. H. J. G. Meijer, T. Munnik, *Annu. Rev. Plant Biol.* **54**, 265 (2003).
19. T. P. Stauffer, S. Ahn, T. Meyer, *Curr. Biol.* **8**, 343 (1998).
20. P. Varnai, T. Balla, *J. Cell Biol.* **143**, 501 (1998).
21. K. Hirose, S. Kadowaki, M. Tanabe, H. Takeshima, M. Iino, *Science* **284**, 1527 (1999).
22. M. S. Nash, K. W. Young, R. A. Challiss, S. R. Nahorski, *Nature* **413**, 381 (2001).
23. P. J. Bartlett, K. W. Young, S. R. Nahorski, R. A. Challiss, *J. Biol. Chem.* **280**, 21837 (2005).
24. B. Mueller-Roeber, C. Pical, *Plant Physiol.* **130**, 22 (2002).
25. Z.-M. Pei *et al.*, *Nature* **406**, 731 (2000).
26. J. I. Schroeder, J. M. Kwak, G. J. Allen, *Nature* **410**, 327 (2001).
27. S. B. McLaughlin, R. Wimmer, *New Phytol.* **142**, 373 (1999).

28. We thank E. Johannes and N. Allen for $PH_{PLC\delta}$-GFP analysis; M. Knight and C. Plieth for aequorin-expressing seeds and vectors; M. Iino for the *$PH_{PLC\delta}$-GFP* clone; A. Webb, M. Knight, C. Plieth, and C. Johnson for advice concerning aequorin imaging; D. Hui for ANOVA analyses; C. Lin and X. Yu for discussions; and J. Siedow, T.-p. Sun, P. Benfey, and X. Dong for supporting ChemioPro system and reading the manuscript. R.-H.T. was supported by a Hargitt fellowship, H.Z. by Xiamen University (NCETXMU) and the Chinese Scholar Council, and C.W.C. by the Andrew Mellon Foundation. This work was supported by grants from the NSF (MCB-0451072) and U.S. Department of Agriculture (CSREES-2005-35304-16196) and by a Zhu Chongshi Presidential Award from Xiamen University (to Z.-M.P.).

Supporting Online Material

www.sciencemag.org/cgi/content/full/315/5817/1423/DC1
Materials and Methods
SOM Text
Figs. S1 to S4
References

29 August 2006; accepted 5 February 2007
10.1126/science.1134457

Odor Cues During Slow-Wave Sleep Prompt Declarative Memory Consolidation

Björn Rasch,[1]* Christian Büchel,[2] Steffen Gais,[1] Jan Born[1]*

Sleep facilitates memory consolidation. A widely held model assumes that this is because newly encoded memories undergo covert reactivation during sleep. We cued new memories in humans during sleep by presenting an odor that had been presented as context during prior learning, and so showed that reactivation indeed causes memory consolidation during sleep. Re-exposure to the odor during slow-wave sleep (SWS) improved the retention of hippocampus-dependent declarative memories but not of hippocampus-independent procedural memories. Odor re-exposure was ineffective during rapid eye movement sleep or wakefulness or when the odor had been omitted during prior learning. Concurring with these findings, functional magnetic resonance imaging revealed significant hippocampal activation in response to odor re-exposure during SWS.

Sleep facilitates the consolidation of newly acquired memories for long-term storage (*1*–*3*). The prevailing model assumes that this consolidation relies on a covert reactivation of the novel neuronal memory representations during sleep after learning (*3*–*6*). In rats, hippocampal neuronal assemblies implicated in the encoding of spatial information during maze learning are reactivated in the same temporal order during slow-wave sleep (SWS) as during previous learning (*7*, *8*). The consolidation of hippocampus-dependent memories benefits particularly from SWS (*9*–*11*), and reactivation of the hippocampus in SWS after spatial learning has also been seen in humans observed with positron emission tomography (*12*). However, none of these studies experimentally manipulated memory reactivation during sleep. Therefore, its causal role in memory consolidation is still unproven.

We used an odor to reactivate memories in humans during sleep, because odors are well known for their high potency as contextual retrieval cues not only for autobiographic memories, as delicately described in Marcel Proust's *Remembrance of Things Past*, but also for various other types of memory, including visuospatial memories (*13*, *14*). Notably, in the brain, primary olfactory processing areas bypassing the thalamus project directly to higher-order regions, including the hippocampus (*15*), which enables them to modulate hippocampus-dependent declarative memories (*16*). The use of olfactory stimuli for cueing memories during sleep is particularly advantageous because odors, in contrast to other stimuli, can be presented without disturbing ongoing sleep (*17*).

To establish a robust association between learning stimuli and a smell, we applied a purely olfactory stimulus (the smell of a rose) (*18*) repetitively while volunteers ($n = 18$) learned object locations in a two-dimensional (2D) object-location memory task in the evening before sleep. During the first two periods of subsequent SWS, the odor was presented again (in an alternating 30 s on/30 s off mode). In a control condition, odorless vehicle was delivered. The object-location task required visually learning the locations of 15 card pairs on a computer screen to a criterion of 60% correct responses (Fig. 1A). The task is sensitive to the memory-improving effect of sleep (*18*) and involves hippocampal function (*19*).

At retrieval testing after sleep, memory of the card locations was distinctly enhanced when the odor had been presented during SWS as compared to presentation of the vehicle alone. After the odor night, participants remembered 97.2 ± 4.1% of the card pairs they had learned before sleep, but they remembered only 85.8 ± 3.8% after the vehicle night ($P = 0.001$; Fig. 2A,

[1]Department of Neuroendocrinology, University of Lübeck, Ratzeburger Allee 160/23a, 23538 Lübeck, Germany. [2]NeuroImage Nord, Department of Systems Neuroscience, University Medical Center Hamburg-Eppendorf, Martinistrasse 52, 20246 Hamburg, Germany.

*To whom correspondence should be addressed. E-mail: born@kfg.uni-luebeck.de (J.B.); rasch@kfg.uni-luebeck.de (B.R.)